Compositional and Physical Results for Rosetta's New Target Comet 67P/Churyumov-Gerasimenko from Narrowband Photometry and Imaging

David G. Schleicher

Lowell Observatory
1400 W. Mars Hill Road
Flagstaff, Arizona 86001

The Lowell Observatory Preprint Series

Compositional and Physical Results for Rosetta's New Target Comet 67P/Churyumov-Gerasimenko from Narrowband Photometry and Imaging

David G. Schleicher

Lowell Observatory, 1400 W. Mars Hill Road, Flagstaff, AZ 86001
email: dgs@lowell.edu

Abstract

We present compositional and physical results of Comet 67P/Churyumov-Gerasimenko, the new target of ESA's Rosetta mission. A total of 16 nights of narrowband photometry were obtained at Lowell Observatory during the 1982/83 and 1995/96 apparitions, along with one night of imaging near perihelion in 1996. These data encompass an interval of -61 to $+118$ days from perihelion, corresponding to a range of heliocentric distances before perihelion from 1.48 to 1.34 AU, and an outbound range from 1.30 to 1.86 AU. Production rates were determined for OH, NH, CN, C_3, and C_2, along with $A(\theta)f\rho$, a proxy of the dust production. Water production, based on OH, has a steep (~ -5) power-law r-dependence post-perihelion and the minor species are somewhat less steep (~ -3 to -4), while the dust is quite shallow (~ -1), possibly due to a lingering population of large, slow-moving grains. All species exhibit larger production rates after perihelion, with water having a $\sim 2\times$ pre/post-perihelion asymmetry, while minor species and dust have larger asymmetries. These asymmetries imply a strong seasonal effect and probable high obliquity of the rotational axis, along with one or more isolated source regions coming into sunlight near perihelion. Peak water production (which occurred about 1 month after perihelion) was $\sim 8 \times 10^{27}$ mol s^{-1} and, when combined with a standard water vaporization model, implies an effective active area on the surface of the nucleus of ~ 1.5-2.2 km^2 or an active fraction of only about 3-4%. Abundances of carbon-chain molecules yield a classification of slightly "depleted" in the A'Hearn et al. (1995, Icarus 118, 223-270) database. The peak dust production (as measured by $A(\theta)f\rho$, and uncorrected for phase angle) was ~ 450 cm, while the color of the dust is moderately reddened, and the mean radial profile has a power-law slope of -1.3. Large night-to-night variability is also present, presumably due to the source region(s) rotating in and out of sunlight along with effects due to the use of differently-sized apertures. A strong sunward radial feature was detected in images obtained near perihelion, along with a significant asymmetry between the two perpendicular directions from the sun/tail line. These features may be the result of a mid-latitude source region sweeping out a cone with each rotation, which we are viewing from the side and where the sunward radial feature is one edge of the cone seen in projection. When combined with other constraints on the pole orientation, a possible pole solution is found having an obliquity of about 134° at an RA of about 223° and a Dec of $-65°$, with a source region located near $+50°$ and in overall agreement with the photometric results. In comparison to the original Rosetta target Comet 46P/Wirtanen, Comet Churyumov-Gerasimenko has essentially the same peak water production but a peak dust production about $3\times$ greater than does Wirtanen based on $A(\theta)f\rho$ (i.e., if one assumes that the properties of the dust grains are similar) (cf. Farnham and Schleicher (1998, A&A 335, L50-55).

Keywords: Churyumov-Gerasimenko, Comets, Photometry, Composition, Coma

1   Introduction

In 1969, Comet 67P/Churyumov-Gerasimenko was discovered shortly after reaching a perihelion distance of 1.28 AU. This was only the second apparition following a major perturbation of its orbit by Jupiter in 1959, prior to which its perihelion distance had been greater than 2.7 AU. Additionally, an earlier perturbation with Jupiter occured in 1840 (Carusi et al. 2005), but the orbit prior to this encounter is not well determined (G. Valsecchi, personal comm.). Therefore, one cannot use orbital dynamics to determine whether Churyumov-Gerasimenko is more or less evolved than other Jupiter-family comets.

Most recently, Comet Churyumov-Gerasimenko (C-G) has become notable because, following the launch postponement of ESA's Rosetta spacecraft scheduled to rendezvous with Comet 46P/Wirtanen, C-G was selected as the new target. The Rosetta spacecraft was successfully launched on 2004 March 2, and is now scheduled to intercept C-G in 2014 May at a heliocentric distance of 4.5 AU, or 15 months prior to perihelion. Following the rendezvous, it is planned that Rosetta will be manuevered to within 200 km of the nucleus, and slowly back off as C-G becomes more active during its approach to the Sun. A probe will also be released to land on the surface of the nucleus early in the mission, when the comet is still expected to be relatively inactive.

For such an ambitious and expensive project – Rosetta was one of ESA's Cornerstone missions begun in the early 1990s – it was important to determine the suitability of C-G and several other candidate comets as viable replacement targets as soon as possible after the postponed launch in early 2003. To this end, we provided a brief summary of results based on our photometric observations from previous apparitions to the Rosetta team in 2003 February, and subsequently Churyumov-Gerasimenko was selected as the new Rosetta target. A more complete summary of our results was also presented at the 2003 DPS meeting (Schleicher and Millis 2003). The choice of C-G as the new Rosetta target also prompted a flurry of new observations, although C-G was outbound and more than 2 AU from the Sun in 2003 (cf. Lamy et al. 2003; Reach et al. 2003; Kidger 2003; Weiler et al. 2004; Schulz et al. 2004; Moreno et al. 2004). Finally, new analyses of older data sets have also recently been published (Weiler et al. 2004; Feldman et al. 2004; Mäkinen 2004; Fulle et al. 2004; Chesley 2004; Davidsson and Gutiérrez 2005; Ferrín 2005).

Our primary data set consists of aperture photometry using narrowband filters obtained at two apparitions: 1982/83 and 1995/96. These observations were acquired as part of our long-term program to determine the chemical composition and physical properties of comets (cf. A'Hearn et al. 1995). This homogeneous database also permits the placement of much more detailed studies obtained from spacecraft, such as Rosetta, into a much broader context and appropriately generalized to other comets. Measurements of key species (OH, CN, and dust) in Churyumov-Gerasimenko obtained on 9 nights during the 1982/83 apparition were published by Osip et al. (1992) as one of nine Jupiter-family comets considered as possible spacecraft targets. Among other conclusions, Osip et al. noted that C-G exhibited significant asymmetry in both the dust and gas production rates, with peak productivity occuring in the month after perihelion, and that the measured dust-to-gas ratio was not only greater than for any other candidate, but also larger than 1P/Halley; however, the absolute dust production was more than a factor of 40 smaller than Halley's. This original data set was supplemented during the 1995/96 apparition, when photometry was obtained on 6 nights, providing both an overlap in orbital coverage and extending the range of pre-perihelion observations by one month. In addition, imaging was obtained through several filters on 1996 January 25, just one week following perihelion.

In this paper, we present all of our photometric measurements from both apparitions, along with the associated production rates. Abundance ratios, peak production rates, and the implied effective active area on the nucleus are given and compared to the original Rosetta target, Comet

46P/Wirtanen. The likely causes of the observed production rate asymmetry near perihelion, the late occurrence of peak production, and the large amount of dispersion among data points are discussed. Coma morphology shortly after perihelion are also presented, along with a plausible, self-consistent model for the nucleus orientation and source location, and other consequences of these results to the Rosetta mission.

2   Observations and Reductions

All observations were obtained from Lowell Observatory's Anderson Mesa site located near Flagstaff. Three telescopes were used at various times: the Perkins 72-inch (1.8-m), the Hall 42-inch (1.1-m), and the 31-inch (0.8-m). A single-channel photoelectric photometer with pulse counting electronics was used for all photometric measurements, while a TI 800^2 CCD was used for the one night of imaging. Following 2×2 on-chip binning, this chip had a resulting pixel scale of 0.724 arcsec/pixel with a field of view of about 4.8 arcmin. In Table 1, we list the observing circumstances for each night, including heliocentric distance, r_H, geocentric distance, Δ, phase angle, θ, and time from perihelion, ΔT.

During the 1982/83 apparition, the original A'Hearn and Millis (AM) set of narrowband comet filters was used. At that epoch, the set consisted of filters isolating emission from the OH, NH, CN, C_2, and C_3 gas molecules, along with continuum filters located at 3675 and 5240 Å. In 1995/96, we were using the International Halley Watch (IHW) filters, which also isolated OH, CN, C_2, and C_3, along with continuum points at 3650 and 4845 Å. In addition, we continued to use the original AM filter isolating the NH emission band, but due to a gradual ongoing degradation of the filter, a linearly interpolated correction factor of 1.68 was automatically applied to these data. In conjunction with the introduction of a new filter set in 1997 for Comet Hale-Bopp (1995 O1), an improved methodology was developed for the removal of contamination of the continuum filters by the wings of known emission bands (Farnham et al. 2000). In addition, improved knowledge of the C_2 and C_3 band shapes has yielded revised coefficients for each of the filters' fractional band transmissions, while a better model was determined for the telluric ozone contribution to the non-linear extinction at the OH filter in the near-UV. These new methodologies have now been back applied to the AM and IHW filter sets, and the equations and coefficients for calibrations and reductions are given in the Appendix of Farnham and Schleicher (2005).

Our one night of imaging obtained on 1996 January 25 includes 2 sets of images guided at the comet's rate of motion, with each set consisting of a V and Kron-Cousins R wide-band filters along with the narrowband C_2 and 4845 Å continuum filters. Signal-to-noise per pixel for the narrowband frames was poor, preventing any useful studies besides gross morphologies. Furthermore, the night was non-photometric, so no standard stars were measured. Frames were bias-subtracted and flat-fielded using standard procedures, then sky-subtracted and each pair of images for a given filter co-added.

As detailed in A'Hearn et al. (1995), our normal procedures were used to obtain all of the photometric observations: Each data set consists of several measurements with each filter, typically totalling 30-120 s of integration, both of the comet centered in the aperture and of a sky location >10 arcmin from the comet. Because of the general faintness of C-G, along with several other comets being targets, only one or at most two sets for C-G were obtained each night. Aperture diameters varied from 7 to 110 arcsec, with most of the small aperture measurements taken in 1982/83. The aperture size used for each data set, along with the associated log of the projected aperture radius in kilometers, ρ, are listed in Table 2. Comet standard stars were measured each night to obtain extinction and instrumental calibrations for each filter, and these were used to reduce the comet

3

observations to absolute fluxes using the revised filter coefficients already discussed (cf. Farnham et al. 2000; Farnham and Schleicher 2005).

Additional reductions to column abundances and production rates for the gas species and to the quantity $A(\theta)f\rho$, a proxy for dust production, also follow our usual procedures detailed in A'Hearn et al. (1995). Fluorescence efficiencies, tabulated in A'Hearn et al. and references therein, are applied to compute the number of molecules within the column defined by the photometer's entrance aperture. Because the fluorescence efficiencies, L/N, for OH, NH, and CN vary with heliocentric velocity and, for CN, with heliocentric distance due to the Swings effect, the specific values are tabulated in Table 1. In Table 2 are listed the resulting column abundances, $M(\rho)$, and these are then extrapolated to total coma abundances by application of a standard Haser model. In particular, the Haser model is used to simply compute the fraction of molecules expected to be contained within the column, assuming the Haser scalelengths tabulated in A'Hearn et al. These scalelengths are consistent with the spatial distributions observed in numerous comets, particularly comets with small or moderate water production rates such as C-G, but we have insuffient observations of C-G to directly check these values. Finally, gas production rates, Q, are computed by dividing the total abundances by the assumed lifetime of each observed species. In the case of OH, which has a single parent and reasonably well-determined parent and daughter velocities and lifetimes, a parent production rate is also computed. Here we use the empirical relation determined by Cochran and Schleicher (1993) to compute a vectorial equivalent production rate of water from the Haser model OH production rate (see also A'Hearn et al. 1995 and Schleicher et al. 1998). Production rate results are listed in Table 3, along with the propogated uncertainties based on photon statistics. $A(\theta)f\rho$, our nominal measure of dust production, was first introduced by A'Hearn et al. (1984) and is the product of the dust albedo at a given phase angle with the filling factor and the projected aperture radius. For dust grains gray in color and following a canonical $1/\rho$ projected radial distribution, the resulting value for $A(\theta)f\rho$ will be independent of wavelength and aperture size. These results are also given in Table 3.

3   Production Rates and Composition

3.1   Overview

We first examine the overall behavior of Churyumov-Gerasimenko's gas and dust production rates, by plotting in Figure 1 the log of each value as a function of the log of the heliocentric distance. Measurements from the two apparitions are distinguished by different symbols, while pre- and post-perihelion data are indicated by using filled and open symbols, respectively. It is immediately evident that all species exhibit higher production rates following perihelion, with OH having a $\sim 2\times$ pre/post-perihelion asymmetry, while minor species and dust have a larger asymmetry, possibly as high as $\sim 8\times$. It also appears that the peak production rates occur approximately 1 month following perihelion, but this is not strongly constrained due to our sampling interval – our observing runs were usually one month apart. Also evident from Figure 1 is the unexpectedly large dispersion among the data points given the generally small individual uncertainties based on photon statistics. As we will discuss in detail a few paragraphs later, we believe that this large dispersion is a direct consequence of rotational variability.

3.2   Heliocentric Distance Dependence

These data of C-G encompass a range of heliocentric distances before perihelion from 1.48 to 1.34 AU and an outbound range from 1.30 to 1.86 AU. Simple linear, least-squares fits to all data points

results in power-law slopes ranging from a low of -0.6 for the green continuum to a high of -5.2 for OH; however, given the large asymmetry about perihelion observed in the production rates of every species, the overall slopes are not particularly useful. Very steep slopes, between -7 and -18, are computed if only the pre-perihelion data points are included, but these each have large formal uncertainties due to the very limited heliocentric distance range, and even larger uncertainties if the data points are affected by rotational variability. To somewhat improve the slope determinations for C-G as it approaches the Sun, we can also include the pair of data points obtained only three days after perihelion, because these perihelion points are generally consistent with a simple power-law fit with the pre-perihelion points. Doing so yields the slopes listed in Table 4, with OH now having the shallowest slope of -6.4 and NH the steepest at -16.4, but still with formal uncertainties in each slope of 2 or more.

The situation following perihelion is significantly better due to the much larger range of heliocentric distance coverage, although still complicated because the peak production does not occur at perihelion but rather about a month later. Including all post-perihelion data, slopes vary from -0.4 for the green continuum to -5.4 for OH (see Table 4). Excluding the pair of data points obtained three days following perihelion (prior to the peak in production rates) has almost no effect on the resulting slopes for the three carbon-bearing species, but slopes for OH, NH, and the continuum are each approximately 1.1 steeper (again see Table 4).

Overall, the nature of C-G's photometric behavior – a continued increase in gas and dust production to a peak about a month following perihelion, and a large pre/post-perihelion asymmetry – is consistent with several other comets which have exhibited strong seasonal variations. The most notable recent example is Comet 19P/Borrelly (Schleicher et al. 2003), except that the sense of the asymmetry and the time of peak production are both reversed from C-G. In any case, with a peak in production occuring away from perihelion, one should use considerable caution if one wishes to extrapolate the derived r_H-dependencies to much larger heliocentric distances, particularily before perihelion. We will return to this topic in Sections 4 and 5.

3.3 Rotational Variability

To better examine the characteristics of the apparent large scatter in the data, we replot the log of the production rates for each species in Figure 2, but now as a function of time from perihelion. In spite of the general scatter, it is evident that when two data sets were obtained on the same night, as was the case for each of the first 4 nights of observations following perihelion, there is generally good agreement between each nightly pair of data points. At the same time, there is clear evidence for significant night-to-night variability in production. In particular, two data sets were obtained on each of three consecutive nights – 1982 Dec 12-14 – with values between adjacent nights differing by as much as a factor $\sim$3. Because, except for the lone case of NH on the middle night, each nightly pair is self-consistent, we consider this strong evidence for intrinsic variability. The different characteristics on these three nights among the different species is also consistent with the variations one might expect due to a source turning on and off with rotation coupled with differing parent lifetimes. As we observed in 1P/Halley (Schleicher and Millis 1989) and Levy (1990c) (Schleicher et al. 1991), rotational lightcurves of coma species vary in amplitude and phase lag due to the respective parent lifetime and the size of the aperture.

Because the derived production rates are computed using a static model, such rates do not represent a measure of the instantaneous release of material from the nucleus when short-term variability is present. Instead, the derived rates represent a time-average of all material currently within the column defined by the aperture size. With aperture radii ranging between $1.0{\times}10^3$ to $5.6{\times}10^3$ km in 1982 December, most material, including daughter products, will move out of the

aperture within several hours of being released from the nucleus. But the rate of response of column abundances (and the resulting derived production rates) to changes in the actual release of material from the nucleus can differ by even longer time scales among the observed species. For instance, C_3 responds very rapidly due to its short-lived parent(s), while species originating from grand-parents generally exhibit phase lags of several hours or more. Further complicating the situation is that larger apertures contain progressively more "old" material, diluting the amplitude of the observed lightcurve caused by the intrinsic production rate changes on the nucleus.

One can ask if the different behavior exhibited by each species observed on these three consecutive nights is reasonable given the rotation period of 12.3±0.27 hr recently determined by Lamy et al. (2003) using the Planetary Camera on the Hubble Space Telescope (HST). Since the night-to-night variations we measured are sometimes as great as ~3×, it is unlikely that these production rate variations are caused simply by the changing cross-section of an elongated nucleus, such as Lamy et al. observed in their double-peaked lightcurve of C-G. Nor would simple cross-sectional area variations explain the large pre-/post-perihelion asymmetry. Instead, one or more isolated source regions turning on and off as it rotates into and out of sunlight can explain both the short-term variability and, with a seasonal change in sub-solar latitude, the asymmetry about perihelion. We would, therefore, expect that an individual source region would produce a *single-peaked* lightcurve with Lamy et al.'s period of 12.3±0.27 hr, while multiple sources could produce more complicated lightcurves.

Based on this period, data on the first two nights, December 12 and 13, have nearly the same rotational phase, while data on December 14 was obtained about 1/3rd of a rotational cycle later. In this scenario, the apparent decrease in computed production rates observed for some species from the 12th to the 13th, most notably CN and C_3, can be attributed to the smaller apertures used on the 13th coupled with the source region(s) having turned off after rotating out of sunlight. Since C_3 has the shortest-lived parent lifetime of the observed species, small-aperture measurements of C_3 are most diagnostic of the instantaneous conditions of the source region, while the larger aperture C_3 measurements yield constraints on the source region activity up to a few hours earlier. In comparison, OH shows no change while C_2 has a larger derived production rate in the smaller aperture, consistent with having a longer-lived parent and having one or more grandparents, respectively. Generally, this pattern of behavior is reminiscent to that exhibited in Halley's rotational lightcurve, portions of which were examined by Schleicher and Millis (1989) for trends with aperture size at different rotational phases.

By the last of the three consecutive nights in December, one-third of a rotational cycle later than the first two nights, the production rates for every species except for C_2 are substantially larger than on the 2nd night, again consistent with C_2 showing a considerable phase lag compared to the other species. A further check on short-term variability can be extracted from the production rates tabulated by Cochran et al. (1992). Here, too, large day-to-day variations by up to a factor of 3 in derived production rates are evident, and again by differing amounts for each species. Taken together, we believe we have a strong, self-consistent case for large-scale rotational variability in Comet Churyumov-Gerasimenko, but full rotational coverage of coma abundances should be obtained during C-G's next apparition in 2009 to confirm this scenario.

An unfortunate consequence of large rotational variability is that, except for the three consecutive nights in 1982 December, we have no way to determine the rotational phase of individual data points. Given the large size of the rotational variations, it is therefore nearly impossible to directly investigate possible changes in production rates between the two apparitions. No obvious difference with apparition is evident for any of the gas species. In contrast, the derived dust production rates do appear to be systematically lower in 1995/96, but as we discuss later in Section 4, this difference is much more likely to be a consequence of the larger aperture sizes predominantly used in the

1995/96 apparition, coupled with the relatively steep radial distribution of dust.

3.4 Composition and Taxonomy

Relative abundances, based on the mean of the log of each production rate ratio of a given species with respect to OH, are presented in Table 4. While the ratios have unusually large uncertainties, these are again a direct result of the rotational variability just discussed and the differing effects of small apertures and phase lags for each species. In fact, as an example, the full range of C_2-to-CN ratios for all data points is displayed just within the three consecutive nights of data from 1982 December. No trends with time nor with heliocentric distance are evident. The average of the log of the C_2-to-CN production rate ratio is -0.21 ± 0.27, or about a factor of 2.2 smaller than the approximate mean value for comets classified as "typical" based on the A'Hearn et al. (1995) classification system. Note that, as discussed in more detail in recent papers (Schleicher and Osip 2002; Schleicher et al. 2003; Farnham and Schleicher 2005), improved understanding in the extent and shape of the wings of the C_2 and C_3 emission bands has resulted in revised reduction coefficients for these filters, on average yielding a slightly increased C_2-to-CN ratio of about 17% (although the specific increase depends on the dust-to-gas ratio of each comet). Since the C-G data have been reduced with these new coefficients, we have also adjusted the "typical" value of $+0.06$ from A'Hearn et al. upwards to $+0.13$ and the somewhat arbitrary division between the typical and depleted classes to -0.11. Therefore, the value of -0.21 for this ratio in C-G implies an approximate depletion by a factor 2.2 of C_2 with respect to CN, or what we would characterize as mildly depleted (given that the range for depleted comets encompasses depletion factors of between 1.7 and 18).

The only other published compositional measurements for C-G which we are aware are those by Cochran et al. (1992), Weiler et al. (2004), and Schulz et al. (2004). As already discussed, the Cochran et al. observations also show large variations in production rates from one night to another, presumably again due to rotational phase lag effects. In fact, for the 5 nights at which C_2 was successfully measured, the C_2-to-CN production rate ratio varies by nearly a factor of 3. This rotationally-induced dispersion, coupled with the usual issues of differing scalelengths used by different researchers in the modeling to compute production rates (cf. Fink and Combi 2004), makes a direct comparison of abundance ratios nearly meaningless. We do note that the straight average of the five nights with measured ratios from Cochran et al. yields a value for C-G about 30% less than the average ratio for the 17 comets included in Cochran et al.'s sample, but about one-quarter of the comets making up their ensemble average are classified as "depleted" by A'Hearn et al. (1995). Therefore, C-G has a lower than average abundance of C_2 in the Cochran et al. sample, but the specific amount of the depletion is uncertain. Weiler et al. (2004) measured a CN production rate of $1.35\pm0.35\times10^{25}$ mol s^{-1} on 1996 Feb 10/11, just slightly higher than our values 2 weeks later. Although C_2 was outside of their spectral coverage, they tentatively identified the C_3 band. We confirm this identification of the C_3 emission band based on the location and relative intensities of 6 features between 3960 and 4120Å in both their continuum subtracted spectrum and in an essentially pure emission spectrum of Comet 122P/deVico obtained by A. Cochran (Farnham et al. 2000). However, their upper limit for the C_3 production rate, 1×10^{25} mol s^{-1}, does not provide a significant constraint on the C_3-to-CN abundance ratio. Finally, Schulz et al. (2004) obtained spectra of C-G in 2003 at heliocentric distances between 2.3 and 2.9 AU. Based on their CN detections and the associated upper limits for C_2, they indicate that C-G was at least slightly depleted at 2.9 AU, while the results at smaller r_H are non-constraining.

The log of the mean dust-to-gas ratio for C-G is -25.27 cm s molecule^{-1}, based on the log of the ratios of $A(\theta)f\rho$ for the green continuum vs Q(OH). This value is essentially identical to the

mean value for the recent Stardust target 81P/Wild 2 of -25.28 (Farnham and Schleicher 2005). As with Wild 2, C-G is dustier than the average of all comets from the A'Hearn et al. (1995) database (which vary over more than 2 orders of magnitude), but in the mid-range of comets in the carbon-chain depleted class. However, unlike for Wild 2 where no trend with distance was evident, there is a significant trend with heliocentric distance in C-G following the time of peak production, as would be expected from the quite different post-perihelion r_H-dependencies for OH and for dust as previously discussed. By the most distant observations, the measured log of the dust-to-gas ratio increases to a value of -24.74, nearly a factor of 4 greater than the mean value. Moreover, if the post-peak production observations ($>+40$ days from perihelion) are excluded from the average, then the average log of the dust-to-gas ratio drops to -25.41, and the post-perihelion large r_H value is nearly a factor of 5 greater than earlier in the apparition. This is clearly well beyond the change which might be attributed to rotation and/or aperture effects (discussed in Section 4).

We believe the most likely explanation for a much shallower r_H-dependence of the dust as compared to gas following perihelion is the lingering presence of a significant population of large, very slowly moving grains. (A basic decrease in dust outflow velocity with distance, due either to lower gas outflow velocities or lower gas production rates, is ruled out because this scenario requires that the dust also have a shallower r_H-dependence than does water before perihelion, opposite of what we observe. The same scenario was invoked by Schleicher et al. (2003) in the case of Comet 19P/Borrelly, as they noted the difficulty in explaining this type of behavior unless a significant population of large, slow-moving grains had been released or a major change in grain properties took place during the apparition. Presumably released from the nucleus in the few months surrounding peak water production – the only time when the gas flow is high enough to lift the more massive grains – such long-lived grains would provide an ever-increasing proportion of the reflected light as the release of grains dropped with decreasing water production and the smaller grains were dispersed. Therefore, this directly implies that the derived $A(\theta)f\rho$ values would no longer be representative of the actual ongoing release of dust in the months following peak production, but would instead be biased by the ever-increasing proportion of reflected continuum radiation from large, older grains. Several characteristics, including the long-term evolution of the coma morphology in Borrelly, further supported their large grain hypothesis (see Schleicher et al. 2003 for detailed discussion). For C-G, large, very-slow moving grains again provide the simplest explanation, and this concept is supported by recent modeling of the dust tail by Fulle et al. (2004) and Moreno et al. (2004), with both groups claiming a much larger population of mm and cm sized grains than most short-period comets. Unexpectedly, model results from both groups indicate that large grains were emitted at a sustained high level beginning many months prior to perihelion, and with significant drop-off of large grain production occuring 1-3 months following perihelion. While the time of drop-off roughly coincides with the drop in water production, the sustained high dust production of large grains prior to perihelion is inconsistent with the measured seasonal behavior of the water production.

This apparent contradiction might be explained by a large heterogeneity among source regions in the particle size distribution of the dust grains. One might imagine a source region dominated by large grains which is in "summer" as the comet approaches the Sun, and which is no longer exposed to sunlight shortly after perihelion. In this scenario, a much larger source region (or regions) in the other hemisphere dominates the total water production (and the small-sized grain production), producing the observed seasonal asymmetry (see Figure 2), but that this larger source contains little or no large-sized grains. This hypothesis, and the model results of Fulle et al. and Moreno et al. should be readily tested by pre-perihelion dust tail observations during the 2008/09 apparition.

3.5 Water Production

The vectorial-equivalent water production rates have been computed from the Haser OH production rates using the empirical conversion indicated in Section 2. Tabulated in the final column of Table 3 and plotted in Figure 3, these values yield r_H-dependent slopes 0.5 steeper than those presented for OH in Table 4 because of the $r_H^{-0.5}$ factor associated with the r_H-dependence of the nominal gas outflow velocity. It is evident from Table 3 that the peak water production measurement is slightly over 1×10^{28} mol s^{-1}, but that a more meaningful rotationally-averaged value at this same time frame one month following perihelion is about 8×10^{27} mol s^{-1}. If we assume that a source region is turning on and off due to rotation, the size of the source region required to produce this average value can to first-order be approximated in the Cowan and A'Hearn (1979) water vaporization model with the isotropic source (which assumes that half of the nucleus is inactive at any given moment). This model yields a source size of 2.2 km^2. However, this is likely to be somewhat of an overestimate, since the overall peak gas production (a month after perihelion) probably occurs when the sub-solar latitude is close to the latitude of the source region on the surface of the nucleus, resulting in more efficient vaporization. In this case, we estimate that the actual required source size is more likely to be about 2/3rds of the nominal value, or about 1.5 km^2. We can combine either of these source size estimates with the nucleus radius determination of 1.98 km from Lamy et al. (2003) based on HST imaging to determine a fractional active area of approximately 3-4%.

Other water production measurements for C-G obtained in 1982 include a data point obtained with IUE and reported by Feldman et al. (2004), results from the OH 18-cm radio lines data base of Crovisier et al. (2002), and a [O I] emission measurement by H. Spinrad and reported by Hanner et al. (1985). The [O I] measurement was obtained on 1982 October 15 and yielded an approximate water production rate of 2×10^{27} mol s^{-1}, or a factor of two less than our average value from the following two nights. In comparison, Crovisier et al. report an average value of 9×10^{27}, based on 14 days of observations (October 9 to 25) surrounding these nights. It is worth noting that the Crovisier et al. average is based on one detection with a value of 3×10^{28} mol s^{-1} and 13 3-sigma upper limits ranging between 1×10^{28} and 6×10^{28} mol s^{-1}. The single OH measurement with IUE was obtained a few weeks later, on November 7 ($\Delta T=-5$), and yielded a water production rate of 6.6×10^{27} mol s^{-1} (Feldman et al. 2004). As is evident, there is considerable scatter among these different data points, which is likely due, at least in part, to rotational variability. In any case, our results at this epoch are in the mid-range of these other water production determinations.

During the 1995/96 apparition, apparently only one other set of water production rates were obtained and these have recently been published by Mäkinen (2004). Based on Lyman-α measurements with the SWAN instrument on the SOHO spacecraft, a total of 5 post-perihelion data points were obtained between ΔT of +4 and +61 days, with results ranging between 5.4 and 9.7×10^{27} mol s^{-1}. Here, again, we have good general agreement, although the peak water production rate from SWAN (which is inherently rotationally averaged) is about 20% higher than our rotationally averaged value of 8×10^{27} mol s^{-1}.

3.6 Photometric Constraints on the Pole Orientation and Source Region Location

As noted in the discussion in the previous sub-section, it is likely that the peak water production occurs when the sub-solar latitude is near the latitude of the source region(s). Other characteristics of the photometric observations provide additional, indirect constraints on the location of the source(s) and the orientation of the rotation axis of the nucleus. The large asymmetry in the production rates of all species (2-8×) before and after perihelion, and the time of peak production

(∼1 month following perihelion), both strongly imply a seasonal effect with the dominate source region(s) quickly coming into sunlight near perihelion, i.e., a rapid change in seasons from winter to summer. To have a large seasonal effect also requires a significant tilt of the rotation axis with respect to the orbital plane, probably greater than ∼30° (and, correspondingly, less than ∼150°). These seasonal characteristics also require that the dominant source region is not located on or too close to the equator of the nucleus. In addition, the large day-to-day variations (2-3×) imply a source region (or multiple, smaller sources with similar longitudes) rotating into and out of sunlight, i.e. it also can not be located near either pole. We conclude, therefore, that the dominant source region is probably located at a mid-latitude on the hemisphere rapidly coming into spring at perihelion.

We note that in an analysis of amateur CCD imaging of C-G during 2002/03, Kidger (2003) reports the occurence of a "perihelic outburst," and further notes that similar outbursts at perihelion were observed at previous apparitions. However, it is apparent from an examination of these apparition lightcurves shown by Kidger (2003) and references therein that the data sets can be equally well-matched by a steep but steady increase in brightness from 2-3 months prior to perihelion until about 1 month after perihelion, as shown in the visual lightcurve obtained by C. Morris (Hanner et al. 1985). These data sets also show considerable dispersion, consistent with our hypothesis of large rotational modulation, with some evidence that the dispersion (i.e., the rotational amplitude) was smaller before perihelion.

Finally, we can compute the maximum possible rate of change in the sub-solar latitude on C-G's nucleus near perihelion, as this is simply the rate of change in the true anomaly if the obliquity of the rotation axis is near 90°. For this extreme case, the sub-solar latitude can change by as much as 50° between ΔT of -30 to $+30$ days. If one further supposed that the Sun crossed the equator of the nucleus at perihelion and that the source region was at a latitude of 45°, then at ΔT $= -30$ day the source region would be exposed to sunlight for only about 35% of each rotation cycle with a maximum solar altitude at local noon of only 20°, while by $+30$ day the Sun would be above the source region's horizon for about 65% of each day and the maximum altitude of the Sun would reach 70°. Since such a scenario is more than sufficient to explain the observed production rate asymmetry, these extreme assumptions (such as 90° obliquity) could be relaxed significantly and still reproduce the observations.

4 Dust Properties

4.1 Phase Angle Effects

Our observations of Churyumov-Gerasimenko were made over a moderate range of phase angles, with the large majority of measurements taking place at phase angles between 18 and 38°, with extremes of 13 and 48°. Since we have chosen to not correct the derived $A(\theta)f\rho$ values for phase effects, primarily because such corrections, while non-negligible, would be smaller than the general dispersion in the data due to rotational variability, here we briefly note how such phase corrections would have affected the results presented thus far. If we assume the phase function derived by Schleicher et al. (1998) from Halley measurements, a phase angle correction between the extrema of C-G observations would be 1.78×, i.e., one could increase the dust values at 48° by this factor to correct to the 13° phase angle measurement, or vice versa. Between 18 and 38°, the corresponding maximum correction factor would be 1.41×. Overall, the most significant effect of correcting for phase angle would be to decrease the 1982 December and 1983 January dust values with respect to other measurements. And since these data are at and just following the peak in nominal production, this would result in an even shallower post-perihelion r_H-dependence than determined in Section

3. In turn, this only magnifies the difference between the steep r_{H}-dependencies for all of the gas species and that of the dust, thereby strengthening our case for the presence of larger, slow moving grains.

As mentioned in the previous section, amateur CCD imaging data have been compiled by Kidger (2003) from the 2002/03 apparition. To minimize the effects due to a general lack of standardization, particularly over the course of an entire apparition from multiple observers, brightness measurements have been extracted using a fixed projected aperture diameter of 10^4 km, and the resulting R magnitudes and associated values of $Af\rho$ are presented in Figures 4-6 of Kidger (2003). As he indicates, these data show a systematic decrease from $\Delta T = +40$ to $+125$, then the comet's brightness and $Af\rho$ increase slowly until $+172$, and finally the comet resumes a steady decrease even steeper than the original slope until the data ends near $+282$ day. With of order 100 data points, these characteristics of the post-perihelion lightcurve are well-determined; however, this "late outburst" 4 to 6 months following perihelion, as Kidger describes, appears to actually be caused by basic phase angle effects. In particular, an ephemeris for the 2002/03 apparition reveals that the phase angle of C-G decreases very slowly from 36 to $31°$ during the first time segment ($+40$ to $+125$ day), then decreases rapidly to only $4°$ near $+200$ day, before rising to $19°$ at $+280$ day. Again using the phase angle relation derived for Halley, we would expect that phase effects alone would yield about a $2.2\times$ increase in brightness at minimum phase angle with respect to the baseline values between 31 and $36°$. Furthermore, at small phase angles any dust tail would extend away from the observer on the back side of the comet, thereby contributing to the measured flux in the extraction apertures, similar to what was observed by Schleicher et al. (2002) for Comet LINEAR (2000 WM1). The reported maximum brightness above the baseline trend by Kidger is 4-$5\times$, implying that the total "outburst" was probably caused by near-equal portions of enhanced backscattering at smaller phase angles and a dust tail contribution, although an unusually high backscattering enhancement causing the entire lightcurve brightening at this epoch cannot be ruled out. Since the timing of this episode of brightening nearly exactly coincides with the decreasing phase angle, and the comet's brightness then drops at a rate steeper than the original rate during the interval when the phase angle increases (essentially returning the comet to the original baseline behavior by about $+280$ day), we conclude that the outburst reported by Kidger between ΔT of $+125$ and $+173$ day does not represent a change in C-G's intrinsic behavior but rather is entirely caused by changing viewing geometry.

4.2   Dust Colors

We first examine dust colors in the coma of C-G by plotting in Figure 3 the difference in the log $Af\rho$ values between the green and UV continuum points. No significant trends are evident, either with distance, time, nor apparition. These colors can be converted to percentage reddening per 1000Å, after allowing for the different locations of the band passes between the two filter sets used at the two apparitions. The resulting unweighted average is $30\pm42\%$ per 1000Å, which we would classify as a moderately reddened color for the dust grains. This is completely consistent with the average value of $24\pm1\%$ per 1000Å determined by Storrs et al. (1992) based on 14 nights of spectrophotometry obtained during 1982/83 at a wavelength range of 3700-6400Å. And although Weiler et al. (2004) report a grey ($-0.7\pm5.1\%$ per 1000Å) continuum between 4070 and 4600Å, this value appears to be too small due to contamination by the C_3 band which they tentatively identified and which we confirmed in Section 3.4.

We have also ratioed the V and R band images described in the next section to search for any evidence of color variations with location in the coma. No structures were detectable in the ratio image, implying that dust properties, particularly the particle size distribution, are similar among

each of the morphological structures discussed next. While this might appear to contradict the earlier claims for a population of large, slow moving grains, note that the images were obtained only a week after perihelion and prior to peak water production, and so more typical micron-sized grains would still be expected to be the dominate source of reflected light from the coma at this time.

4.3   Coma Morphology and Constraints on the Pole Orientation and Source Location

As mentioned previously, we obtained a limited number of images on 1996 January 25, one week following perihelion. In Figure 4 we show the broadband R composite image following an enhancement by removing a $1/\rho$ profile. This filter, with the best S/N, is normally dominated by reflected continuum from the dust, although a small amount of contaminating emission (primarily from NH_2) would also be expected to be present. However, ratioing the R band image to the images in the V band, and to the narrowband C_2 and green continuum show no significant differences, indicating that emission, even in the C_2 bandpass, is minimal, presumably because of the high dust-to-gas ratio and the limited S/N in the narrowband filters. Given that the R band has the best S/N and otherwise matches the appearance of the green continuum bandpass, the remaining discussion focuses on the R band image.

Immediately evident from Figure 4 is a strong feature towards the southwest, at a position angle (PA) of about 230-240°. With the Sun at a PA of 248° (and 43° out of the sky plane), this feature, possibly a jet, is apparently emitted from somewhere on the sunward hemisphere of the nucleus. Note that the central condensation or origin is in the center of the figure, precisely at the center of the dark spot. This spot is caused by the combination of seeing blur and the removal of a $1/\rho$ profile which was not smoothed for seeing, therefore removing too much light at the presumed nucleus location. A second, more diffuse feature extends towards the east and is centered at a PA of about 85°. This may be associated with older material within a dust tail, as it is about 17° from the anti-solar direction, and near the expected location of larger grains released 2-5 months previous to the observation (T. Farnham, personal communication). Finally, there is a general asymmetry with more material towards the southeast as compared to the northwest. We note that all of these features are obvious even on the unprocessed R and V frames. Other processing algorithms, besides the $1/\rho$ enhancement used in Figure 4, were tried, but none showed any additional features beyond those just described.

Taking a ratio of the two images obtained with each filter shows no temporal variations in morphology during the ∼25 minutes between frames. This is not too surprising, as this time interval only corresponds to 3% of Lamy et al.'s (2003) rotation period of 12.3 hr. While the feature pointing towards the southwest is nearly linear, a close examination shows a slight clockwise curvature, with the center of brightness at a PA of about 240° at a projected distance of 4000 km, but nearer to 230° at 4 times this distance, or 16000 km. Note that this latter distance is approximately where it begins to become difficult to discern the feature from the background coma. There is also possible evidence of a stair-step type drop of brightness along the southwest feature. We extracted the average radial profile within 10° wedges centered at PAs of both 240 and 230°. Along with a monotonic drop in brightness beyond the peak excess at 4000 km following the removal of the $1/\rho$ profile, steeper drops in the brightness appear to occur at projected distances of about 12×10^3, $17\text{-}19 \times 10^3$, and $24\text{-}25 \times 10^3$ km, or at about 6000-7000 km per "step," each followed by slightly shallower than average decreases (indicated in Figure 5). If real, these "steps" may correspond to consecutive rotational cycles of the nucleus. Again using the rotation period from Lamy et al., this corresponds to a projected velocity of just under 0.2 km s^{-1}. While about a factor of two smaller

than the bulk outflow velocity of grains measured in Comet Hyakutake (1996 B2) by Schleicher and Woodney (2003), this is not an unreasonable value, since it would correspond to a lower limit on the outflow velocity given an unknown projection effect, and because the water production rate was more than an order of magnitude greater in Hyakutake (cf. Schleicher and Osip 2002) as compared to C-G.

Based on the results from the photometric analyses in Section 3, a plausible but not conclusive scenario can be created. Since we have already established the probable existence of an isolated, mid-latitude source region to explain both the seasonal and rotational effects, we can reasonably assume that the feature directed towards the southwest arises from this source. Because the feature appears nearly-linear, rather than as a spiral or a series of arcs, we are probably viewing from the side one edge of the cone swept out by rotation of the jet, rather than viewing from the interior of the cone. We further suppose that the general spatial asymmetry, with the coma significantly brighter in the southeast quadrant as compared to the northwest quadrant, is also due to the swept out cone viewed from the side. In this scenario, the observed southwest feature is actually the edge of the cone (similar to the planetary nebula effect) and at this position angle, the physical jet is rotating towards or away from us, i.e. perpendicular to the sky plane. Each of the brightness steps along the southwest feature would still correspond to succesive rotational cycles. The opposite side of the cone is either not discernable because the Sun is either near or below the horizon when the jet would be at this location, or the fainter feature near 85° is actually the other edge of the cone, rather than being associated with the comet's dust tail (expected to be located near the anti-solar direction of 68°).

This scenario is not the only possible explanation of individual features. For instance, the enhancement towards the east might also be explained by slow moving grains in the tail released between about 2-5 months before perihelion (T. Farnham, personal communication). And the near-linear bright feature towards the southwest could be due to a polar jet, but this would not explain the large day-to-day photometric variability. For these reasons, we prefer the scenario described in the previous paragraph because it provides a self-consistent explanation for the observed coma morphology along with the photometric behavior. This scenario also directly implies that the projected PA of the rotation axis is between about 160° (if the faint eastward feature is the second edge of the cone) and ~200° (if only the enhancement in the southeast-to-southwest quadrant is produced by the source).

Following the completion of our just-described analysis, an additional strong constraint on the pole orientation was published by Weiler et al. (2004). They extracted a series of brightness profiles as a function of position angle from images they obtained in March 2003, and identified two significant radial features in addition to the tail. These features were located at PAs of about 125° and 197° and the authors speculate that these might correspond to the two sides of a side-on, swept-out cone. If true, this directly implies a PA of the pole of about 161°, and an inclination of the projected rotation axis to the orbital plane of about 40° (Weiler et al.). While their derived rotation axis PA matches one extreme of our range of possible pole PAs, this is entirely coincidental, as the viewing geometries were completely different with most of Weiler et al.'s observations taking place more than 7 months following perihelion. In fact, combining their resulting PA for the pole with our range of values provides a strong 3-dimensional constraint on the pole orientation, since each projected pole orientation defines a great circle of solutions which only cross in two regions 180° apart.

We used the Monte Carlo jet model developed by Schleicher and Farnham and described in detail in Schleicher and Woodney (2003), to perform grid-pattern searches for viable pole solutions based on the constraints just discussed. Because our own image yields a range of possible PAs for the pole, a family of solutions results. However, most of these possible pole solutions cannot

simultaneously reproduce the observed jet from both data sets unless different source regions are invoked for the two different times of observations. And while it is not unreasonable to have two sources on the surface, many such scenarios would result in both sources producing jets at each observing window for which there is no evidence. An alternative is to have the two sources in opposite hemispheres, with each one experiencing "winter" at one of the two different times from perihelion. This scenario cannot be ruled out. There is, however, one solution (PA of ∼185°) from our range of possible PAs (∼160-200°) which can successfully reproduce the major morphological features from both data sets using only a single source region:

This "best solution" has a pole obliquity of about 134° and an orbital longitude of the pole of about 188°, corresponding to an RA of about 223° and a Dec of −65°. The source region must be located near +50° and has a radius probably between 15 and 30°. (Note that we have arbitrarily assumed that the northern hemisphere is in summer at peak gas production, but that we have no constraint on the sense of rotation of the nucleus.) As shown in Figure 4, this solution also reproduces the stair-step appearance along the sunward feature in our image using an outflow velocity of between 0.3 and 0.4 km/s, and the bulk brightness asymmetry towards the southeast-to-southwest. The slight clockwise curvature of the near-sunward feature is explained by the effects of radiation pressure, while the eastward brightening might also be due to radiation pressure on the smallest grains in the jet or very slow moving large grains released several months earlier. This best solution also yields a large seasonal effect, with the sub-solar latitude crossing the equator near ∆T of −130 days and +180 days, and reaching a maximum value of +46° about 2 weeks after perihelion. With the source region centered at about +50°, a peak gas production would be expected near this time, just slightly before the observed peak from our photometry, and it is evident that measured production rate behavior as a function of time (see Figure 2) is qualitatively matched by this model solution.

Subsequent to the submission of this paper, two independent investigations of the orientation of the rotational axis were published using a variety of constraints including the water production curve, and non-gravitational variations in C-G's orbit. Chesley (2004), also including the morphology constraints from Weiler et al. (2004), determined a pole orientation having a location of RA = 90° and Dec = +75° with an uncertainty of about 10°, and a source located at a mid-latitude in the southern hemisphere. With no constraint on the sense of rotation, the 180° solution is equally possible, and this is only about 15° from our own solution presented above. Davidsson and Gutiérrez (2005) conducted extensive modeling which yielded regions of viability for the pole orientation depending upon different assumptions. They concluded that both Chesley's solution and our own were within high probability regions (see Davidsson and Gutiérrez for details). Imaging of C-G throughout the upcoming apparition should readily test whether this single source "best solution" is correct, or whether a different answer, perhaps with multiple source regions, is required.

4.4 Radial Distribution of Dust

One dust characteristic briefly mentioned in Section 3 was an apparent overall decrease in derived $A(\theta)f\rho$ values during the 1995/96 apparition as compared to 1982/83. And while the comet's phase angle was generally larger in 1995/96 than in 1982/83, the difference at any particular ∆T from perihelion is not sufficient to explain this trend with apparition. Because none of the gas species exhibited similar behavior, it also seems unlikely that this decrease is a real evolutionary effect. Instead, we note that, on average, much smaller aperture sizes were used in 1982/83 than in 1995/96, and numerous comets have shown trends in derived $A(\theta)f\rho$ values with aperture size. Although we never obtained a wide range of photometric aperture measurements on a single night, we can use our single night of imaging to examine the radial distribution of the dust.

Using the resulting frame from the co-added broadband R images discussed in the morphology section above, we have extracted radial profiles in several directions as well as an azimuthal averaged profile. In Figure 5 we show this average profile, along with radial cuts along the primary, sunward feature (PA=230°), opposite the feature, and perpendicular towards the northwest in a log-log plot. The radial profile along the jet falls off with a slope that starts out at -1.0 and steepens to about -1.6 with increasing distance. The radial profile in the direction opposite the jet falls off steadily with a slope of -1.33, similar to the behavior in all directions between position angles of about $45°$ and $200°$. The steepest radial fall-off occurs towards the northwest, with a slope of about -1.7. The overall average slope is about -1.3.

Given the range of aperture sizes used during the 1982/83 apparition as compared to those used in 1995/96, this average radial profile extracted from the imaging implies an expected decrease of approximately 1.5-2.3× in fluxes and resulting $A(\theta)f\rho$ values between the two apparitions. This result is completely consistent with the apparent overall offset in the derived dust production rates evident in Figures 1 and 2, again implying no evidence for actual differences between these two apparitions.

5 Implications for the Rosetta Mission and Summary

In many respects, Comet Churyumov-Gerasimenko is an ideal candidate for the Rosetta rendezvous mission. It can be considered a "proto-typical" Jupiter-family comet, having a large pre-/post-perihelion asymmetry, steep r_H-dependencies, moderate depletions of C_2 and C_3, and coma morphologies likely due to one or more jets, presumably arising from isolated source regions. Each of these characteristics is exhibited by many if not most comets believed to have originated in the Kuiper Belt. More specifically, C-G exhibits the following compositional and physical properties:

Based on narrowband photometric measurements obtained at two apparitions, we can conclude that gas and dust production peaks approximately 1 month following perihelion, after a near-continuous steep rise in production for several months. Following this peak, production rates drop at a slower but still steep rate, except for the dust. These characteristics are consistent with a seasonal effect caused by one or more major source regions rapidly coming into illumination as the comet approaches the Sun, i.e. changing from winter to spring to summer. This implies a significant obliquity of the rotation axis, and that the rotationally averaged maximum total sunlight at the latitude of the source region(s) must occur approximately 1 month after perihelion. Latitudes near the equator are ruled out since such a location should not be able to produce the very steep pre-perihelion r_H-dependence. Even though C-G's peak production follows perihelion, for several reasons we believe that it is highly unlikely that it is caused by a significant thermal lag. First, comets which show pre-/post-perihelion asymmetries do so with near-equal numbers having higher productions before perihelion as after (A'Hearn et al. 1995). Second, the seasonal model is completely successful in reproducing the behavior of Comet Borrelly. Borrelly displayed many of the same properties as C-G, only in reverse, with peak production preceding perihelion and a steep decline in production following. Moreover, in the case of Borrelly, the pole orientation and source location are known and yield a seasonal model *quantitatively* consistent with the observations (Schleicher et al. 2003). Finally the large short-term variability exhibited by C-G is very likely to be rotationally-induced, as observed in other comets such as Halley (Millis and Schleicher 1986) and Levy (1990c) (Schleicher et al. 1991; Feldman et al. 1992). Such large variations require a rapid response to changes in solar insolation, i.e. a short rather than a long lag time.

Our best estimate for the total size of the source region(s) is about 1.5-2.2 km^2, or only about 3-4% of the total surface area, based on the nucleus radius determined by Lamy et al. (2003). This

directly implies that most of the surface is either inert (possibly crusted over) or releases gas at a much lower rate than computed by a nominal water vaporization model. The large short-term variability – of up to a factor of 3 in amplitude – requires a source region or regions moving into and out of sunlight with the rotation of the nucleus, thereby requiring the source(s) to *not* be located at or near the rotational poles. Taken together, the photometric data strongly suggest the presence of one or more isolated source regions located at mid-latitudes, and that as the comet approaches the Sun, the sub-solar latitude begins in the opposite hemisphere and rapidly approaches that of the source region(s) near and immediately following perihelion.

Our very limited imaging of C-G on one night shortly after perihelion revealed a bright, near-linear feature, close to the PA of the Sun. A fainter, more diffuse linear feature was located towards the east, near the expected tail direction, while a large asymmetry was evident between the two perpendicular directions to the Sun-tail line. No obvious variation of dust color with location in coma was detected. The bright feature is presumably associated with the jet one would expect to be produced from the proposed mid-latitude source region. However, lack of obvious spiral structure implies that this feature is probably one edge of a swept-out cone seen side-on, and that the sub-Earth latitude is closer to the equator than is the source latitude. In this scenario, the asymmetric brightening towards the southeast between the bright feature and near-tailward feature would be the side of the cone, and the step-like brightness fall-off along the primary feature is caused by successive rotational cycles. Less certain is the identification of the near-tailward feature: it might simply be caused by large, slow moving grains in the dust tail released many months prior to perihelion or very light grains pushed rapidly back from the jet by radiation pressure, or it might be the other edge of the side-on cone. In any case, there is clear evidence of directed emission of dust from the nucleus around the time of perihelion which the Rosetta team should take into consideration. A pair of linear features observed by Weiler et al. (2004) in March 2003 also might be the edges of a cone, and if so, strongly constrain the 3-D location of the rotation axis. Our modeling of these morphological features yields a "best" solution with an isolated source region located near $+50°$ latitude on a nucleus having an obliquity of the pole of $134°$ (RA of about $223°$ and a Dec of about $-65°$). This solution also naturally reproduces the seasonal behavior of C-G's production rate as a function of time. However, alternative pole solutions with more than one source region are not ruled out by the existing data sets. The correct nucleus model should be readily determined by extensive monitoring of C-G's coma morphology throughout the upcoming 2008/09 apparition.

The presence of a mostly inert surface along with an isolated source region or regions most likely implies long-term evolution of the surface. However, the only apparent change in photometric behavior between the two apparitions was exhibited by the dust, and this change was completely explained as an artifact caused by a steeper radial profile of the dust than the canonical $1/\rho$ coupled with different-sized photometric apertures used at the two apparitions. Given the same photometric behavior in 1982/83 and in 1995/96, we can conclude that the same sources were active and that the pole orientation was substantially the same over this time interval. It is therefore reasonable to assume that these physical properties of the nucleus will likely still be valid during Rosetta's apparition in 2015.

Although we saw no evidence of variation in the amount of depletion of C_2 and C_3 with respect to CN as a function of time nor heliocentric distance, there was sufficient variation in the r_H-dependencies of water as compared to the minor species to suggest some compositional inhomogeneities across the surface of C-G. This might be due to differing abundances among different source regions, or it might be caused by differing proportions of "leakage" from the overall inert surface as compared to the isolated source(s). Alternatively, it might be associated with changing proportions of carbon-bearing molecules produced by icy grains versus parent gas species. Rosetta

should easily resolve which, if any, of these possibilities is correct.

The measured peak (rotationally averaged) water production rate for C-G was $\sim$8×10^{27} mol s^{-1}, essentially the same as we measured for the original Rosetta target, Comet Wirtanen (cf. Farnham and Schleicher 1997). In contrast, C-G's peak dust production rate (as measured by $A(\theta)f\rho$ and uncorrected for phase angle) was $\sim$450 cm, or about 3× greater than we determined for Wirtanen, assuming the physical properties of the dust grains and the particle size distributions are similar; however, we note that recent analyses by Fulle et al. (2004) and Moreno et al. (2004) imply that C-G has a much larger abundance of large grains than does Wirtanen, and therefore that the particle size distributions might be quite different. Therefore, the stand-off distance of the spacecraft from the nucleus near perihelion might need to be increased significantly over the original plans for Wirtanen, but the two comets are quite similar in many other respects. C-G's peak water and dust production rates are, of course, much smaller than those we measured for Comet 1P/Halley near the time of the Giotto fly-by (cf. Schleicher et al. 1998), with water and dust each smaller by about a factor of 50.

Perhaps our least well known characteristics for C-G are the production rates at larger heliocentric distances, particularly before perihelion. Because our measurements after perihelion extend for 17 weeks or to r_{H}=1.86 AU, extrapolations to larger distances are reasonably secure, if one uses the r_{H}-dependencies determined only from data obtained after peak production (see Table 4). These slopes – with water quite steep, the minor gas species somewhat less steep, and the dust quite shallow – apparently indicate a decreasing amount of total solar illumination beyond that associated with the change in r_{H}, possibly due to a lowering of the sun angle at the latitude of the source(s). However, the shallow slope for the dust is unlikely to be associated with an actual ongoing near-steady level of dust production, as this would require a greater proportion of dust to be released as water production decreases, and the dust must be lifted by the gas. We conclude, therefore, that this is evidence for a substantial population of large, very slow moving grains which linger in the coma, after presumably being released from the nucleus near the time of peak gas production. We note that the "outburst" at larger r_{H} reported by Kidger (2003) can be entirely explained as the combined effects of phase angle effects in the scattering of the grains as C-G approached minimum phase angle along with possible tail contributions at small phase angle. In fact, we see no evidence of any outbursts or sporadic activity; rather, the rapid rise in brightness through perihelion appears to simply be caused by the continued change in available illumination for one or more source regions coming out of winter, while the large short-term variability is very likely due to diurnal effects.

Unfortunately, because of our short observational arc before perihelion, coupled with the very steep r_{H}-dependent slopes for all of the species, it is not prudent to extrapolate these slopes to the large distances which are important for planning the initial Rosetta encounter or the pre-perihelion rendezvous phase. Assuming that the observed production rate behavior is indeed seasonal in nature, then we would *not* expect the very steep slopes to continue to large r_{H} simply because the sub-solar latitude can no longer change rapidly. Fortunately, the observing geometries are very good at C-G's next apparition in 2008/09 for the pre-perihelion time frame, permitting these important data to be obtained prior to the 2014/15 rendezvous.

With the Rosetta spacecraft now successfully launched, we can look forward to the first rendezvous mission with a comet, and it is clear that Comet Churyumov-Gerasimenko provides both a very representative and interesting target. The Rosetta mission promises to produce many "firsts" for cometary science, including watching cometary activity turn on as the nucleus approaches the Sun, and the response of source regions to changing solar insolation with season and with rotation. The entire surface of a nucleus will be mapped in detail for the first time, and a probe will land and directly sample the composition and structure of the surface. In these and other respects,

Rosetta will severely test models of the nucleus, and will likely transform our understanding of Churyumov-Gerasimenko presented here and in other papers.

Acknowledgements

References

A'Hearn, M. F., Millis, R. L., Schleicher, D. G., Osip, D. J., and Birch, P. V. (1995) The Ensemble Properties of Comets: Results from Narrowband Photometry of 85 Comets, 1976-1992. *Icarus* **118**, 223-270.

A'Hearn, M. F., Schleicher, D. G., Feldman, P. D., Millis, R. L., and Thompson, D. T. (1984) Comet Bowell 1980b. *Astron. J.* **89**, 579-591.

Carusi, A., Kresák, L., and Valsecchi, G. B. (2005) Atlas of Dynamical Evolutions of Short-Period Comets. http://www.rm.iasf.cnr.it/ias-home/comet/catalog.html.

Chesley, S. R. (2004) An Estimate of the Spin Axis of Comet 67P/Churyumov-Gerasimenko. *Bull. Amer. Astron. Soc.* **36**, 1118.

Cochran, A. L., Barker, E. S., Ramseyer, T. F., and Storrs, A. D.: 1992, "The McDonald Observatory Faint Comet Survey: Gas Production in 17 Comets." *Icarus* **98**, 151-162.

Cochran, A. L., and Schleicher, D. G. (1993) Observational Constraints on the Lifetime of Cometary H_2O. *Icarus* **105**, 235-253.

Cowan, J. J., A'Hearn, M. F. (1979) Vaporization of comet nuclei – Light curves and life times. *Moon Planets* **21**, 155-171.

Crovisier, J., Colom, P., Gérard, E., Bockelée-Morvan, D., Bourgois, G. (2002) Observations at Nançay of the OH 18-cm lines in comets. The data base. Observations made from 1982 to 1999. *Astron. Astrophys.* **393**, 1053-1064.

Davidsson, B. J. R., and Gutiérrez, P. J. (2005) Nucleus properties of Comet 67P/Churyumov-Gerasimenko estimated from non-gravitational force modeling. *Icarus* **176**, 453-477.

Farnham, T. L., and Schleicher, D. G. (1998) Narrowband Photometric Results for Comet 46P/Wirtanen. *Astron. Astrophys.* **335**, L50-L55.

Farnham, T. L., and Schleicher, D. G. (2005) Physical and Compositional Studies of Comet 81P/Wild 2 at Multiple Apparitions. *Icarus* **173**, 533-558.

Farnham, T. L., Schleicher, D. G., and A'Hearn, M. F. (2000) The HB Narrowband Comet Filters: Standard Stars and Calibrations. *Icarus* **147**, 180-204.

Farnham, T. L., Schleicher, D. G., Williams, W. R., and Smith, B. R. (1999) The Rotation State and Active Regions of Comet Hale-Bopp (1995 O1). *Bull. Amer. Astron. Soc.* **31**, 1120.

Feldman, P. D., A'Hearn, M. F., and Festou, M. C. (2004) Observations of Comet 67P/Churyumov-Gerasimenko with the International Ultraviolet Explorer at Perihelion in 1982. In "The New ROSETTA Targets" (L. Colangeli, E. Mazzotta Epifani, and P. Palumbo, Eds.) Kluwer Academic Publishers, Dordrecht, pp 47-52.

Feldman, P. D., Budzien, S. A., A'Hearn, M. F., Festou, M. C., and Tozzi, G. P. (1992) Ultraviolet and visible variability of the coma of Comet Levy (1990c). *Icarus* **95**, 65-72.

Ferrín, I. (2005) Secular light curve of Comet 28P/Neujmin 1 and of spacecraft target Comets 1P/Halley, 9P/Tempel 1, 19P/Borrelly, 21P/Giacobinni-Zinner, 26P/Grigg-Skjellerup, 67P/Churyumov-Gerasimenko, and 81P/Wild 2. *Icarus* **178**, 493-516.

Fink, U., and Combi, M. R. (2004) The effect of using different scale lengths on the production rates of Comet 46P/Wirtanen. *Planet. Space Sci.* **52**, 573-580.

Fulle, M., Barbieri, C., Cremonese, G., Rauer, H., Weiler, M., Milani, G., and Ligustri, R. (2004) The dust environment of comet 67P/Churyumov-Gerasimenko. *Astron. Astrophys.* **422**, 357-368.

Hanner, M. S., Tedesco, E., Tokunaga, A. T., Veeder, G. J., Lester, D. F., Witteborn, F. C., Bregman, J. D., Gradie, J., Lebofsky, L. (1985) The dust coma of periodic Comet Churyumov-Gerasimenko (1982 VIII). *Icarus* **64**, 11-19.

Kidger, M. R. (2003) Dust production and coma morphology of 67P/Churyumov-Gerasimenko during the 2002-2003 apparition. *Astron. Astrophys.* **408**, 767-774.

Lamy, P. L., Toth, I., Weaver, H., Jorda, L., Kaasalainen, M. (2003) The Nucleus of Comet 67P/Churyumov-Gerasimenko, the New Target of the Rosetta Mission. *Bull. Amer. Astron. Soc.* **35**, 970.

Mäkinen, J. T. (2004) Water production rate of comet 67P/Churyumov-Gerasimenko. In "The New ROSETTA Targets" (L. Colangeli, E. Mazzotta Epifani, and P. Palumbo, Eds.) Kluwer Academic Publishers, Dordrecht, pp 61-67.

Millis, R. L. and Schleicher, D. G. (1986) The Rotational Period of Halley's Comet. *Nature* **324**, 646-649.

Moreno, F., Lara, L. M., Muñoz, O., López-Moreno, J. J., and Molina, A. (2004) Dust in Comet 67P/Churyumov-Gerasimenko. *Astrophys. J.* **613**, 1263-1269.

Osip, D. J., Schleicher, D. G., and Millis, R. L. (1992) Comets: Groundbased Observations of Spacecraft Mission Candidates. *Icarus* **98**, 115-124.

Reach, W. T., Hicks, M. D., Gillam, S., Bhattacharya, B., Kelly, M. S., and Sykes, M. V. (2003) The Debris trail and Near-nucleus Dust Environment of the ROSETTA mission target 67P/Churyumov-Gerasimenko. *Bull. Amer. Astron. Soc.* **35**, 970.

Schleicher, D. G., and Millis, R. L. (1989) Revised Scalelengths for Cometary NH. *Astrophys. J.* **339**, 1107-1114.

Schleicher, D. G., and Millis, R. L. (2003) Results from Narrowband Photometry of ROSETTA's New Target Comet 67P/Churyumov-Gerasimenko. *Bull. Amer. Astron. Soc.* **35**, 970.

Schleicher, D. G., Millis, R. L., and Birch, P. V. (1998) Narrowband Photometry of Comet P/Halley: Variation with Heliocentric Distance, Season, and Solar Phase Angle. *Icarus* **132**, 397-417.

Schleicher, D. G., Millis, R. L., Osip, D. J., and Birch, P. V. (1991) Comet Levy (1990c): Ground-based Photometric Results. *Icarus* **94,**, 511-523.

Schleicher, D. G., and Osip, D. J. (2002) Long and Short-term Photometric Behavior of Comet Hyakutake (1996 B2). *Icarus* **159**, 210-233.

Schleicher, D. G., Woodney, L. M., and Birch, P. V. (2002) Photometry and Imaging of Comet C/2000 WM1 (LINEAR). *Earth, Moon, and Planets* **90**, 401-403.

Schleicher, D. G., Woodney, L. M., and Millis, R. L. (2003) Comet 19P/Borrelly at Multiple Apparitions: Seasonal Variations in Gas Production and Dust Morphology. *Icarus* **162**, 415-

442.

Schleicher, D. G., and Woodney, L. M. (2003) Analyses of Dust Coma Morphology of Comet Hyakutake (1996 B2) Near Perigee: Outburst Behavior, Jet Motion, Source Region Locations, and Nucleus Pole Orientation. *Icarus* **162**, 190-213.

Schulz, R., Stüwe, J. A., and Boehnhardt, H. (2004) Rosetta target comet 67P/Churyumov-Gerasimenko: Postperihelion gas and dust production rates. *Astron. Astrophys.* **422**, L19-L21.

Storrs, A. D., Cochran, A. L., and Barker, E. S. (1992) Spectrophotometry of the Continuum in 18 Comets. *Icarus* **98**, 163-178.

Weiler, M., Rauer, H., and Helbert, J. (2004) Optical Observations of Comet 67P/Churyumov-Gerasimenko. *Astron. Astrophys.* **414**, 749-755.

Figure Captions

Figure 1: Log of the production rates for each observed molecular species and $A(\theta)f\rho$ for the green continuum plotted as a function of the log of the heliocentric distance. Data points from the 1982/83 apparition are shown as triangles while those from 1995/96 are given as circles; filled symbols represent data obtained before perihelion while open symbols are used for post-perihelion measurements. Vertical dotted lines represent perihelion distances, with the larger distance corresponding to both of our observed apparitions while the smaller distance corresponds to the upcoming apparitions in 2009 and 2015 (these 4 perihelion distances monotonically decrease with time). Note the large asymmetries around perihelion for all species, and the much more shallow $r_{\rm H}$-dependence for dust as compared to the gas species following perihelion.

Figure 2: Same as Figure 1, but production rates are plotted as a function of time from perihelion. Here it is evident that the peak production rates for all species are reached about 1 month following perihelion. The large dispersion is apparently due to substantial rotational variability, and the detailed differences among species are consistent with changes in aperture size and phase lags associated with differing lifetimes of parent or grandparent species.

Figure 3: Log of the water production and dust color as a function of the log of $r_{\rm H}$. Symbols are the same as in Figure 1. Vectorial-equivalent water production rates (top) are computed from the Haser OH production rates, overlaid by the curve expected by a basic water vaporization model scaled to the rotationally-averaged peak production rate about 1 month after perihelion. The observed steep production rates are most likely caused by seasonal effects (see text for details). The color of the dust is shown as the differential $A(\theta)f\rho$ between the green and UV. The dust color shows no evidence of trends with heliocentric distance nor with aperture size.

Figure 4: R band composite image of Comet Churyumov-Gerasimenko from 1996 January 25, one week after perihelion (left). As shown, the image is enhanced by dividing by a canonical ρ^{-1} profile to remove the bulk falloff of the coma. The dark spot at the center is the result of seeing blur of the nucleus region followed by the ρ^{-1} removal. North is up, East is to the left, and the field of view corresponds to 6×10^4 km at the comet. The position angle of the Sun ($248°$) and the anti-sunward directions are shown with white PA indicators. The bright, near-linear feature observed towards the position angle of 230-240° (black PA indicator) is believed to correspond to one edge of a side-on

cone swept out by a rotating jet. The faint feature towards the east is likely associated with material swept back into the dust tail (see text for details). Our best synthetic model solution of C-G is shown in the right-hand panel, also with a ρ^{-1} profile removed. The nucleus has an obliquity of the pole of 134° and includes a +50° latitude source region which reproduces the bright jet and the bulk asymmetry towards the southeast-to-southwest. This solution (see Section 4.3) also produces a side-on cone which matches the location of a pair of radial features observed by Weiler et al. (2004) in March 2003.

Figure 5: Surface brightness profiles for the image shown in Figure 4. Profiles along the primary jet (PA=230-240°), opposite of the jet, and perpendicular to the jet towards the northwest are shown, along with the azimuthal averaged profile, which has a slope of about −1.3 (see Section 4.4 for details). Arrows indicate positions of steeper drops along the primary jet (solid), which are each followed by a shallower sections, possibly associated with successive rotational cycles (see Section 4.3).
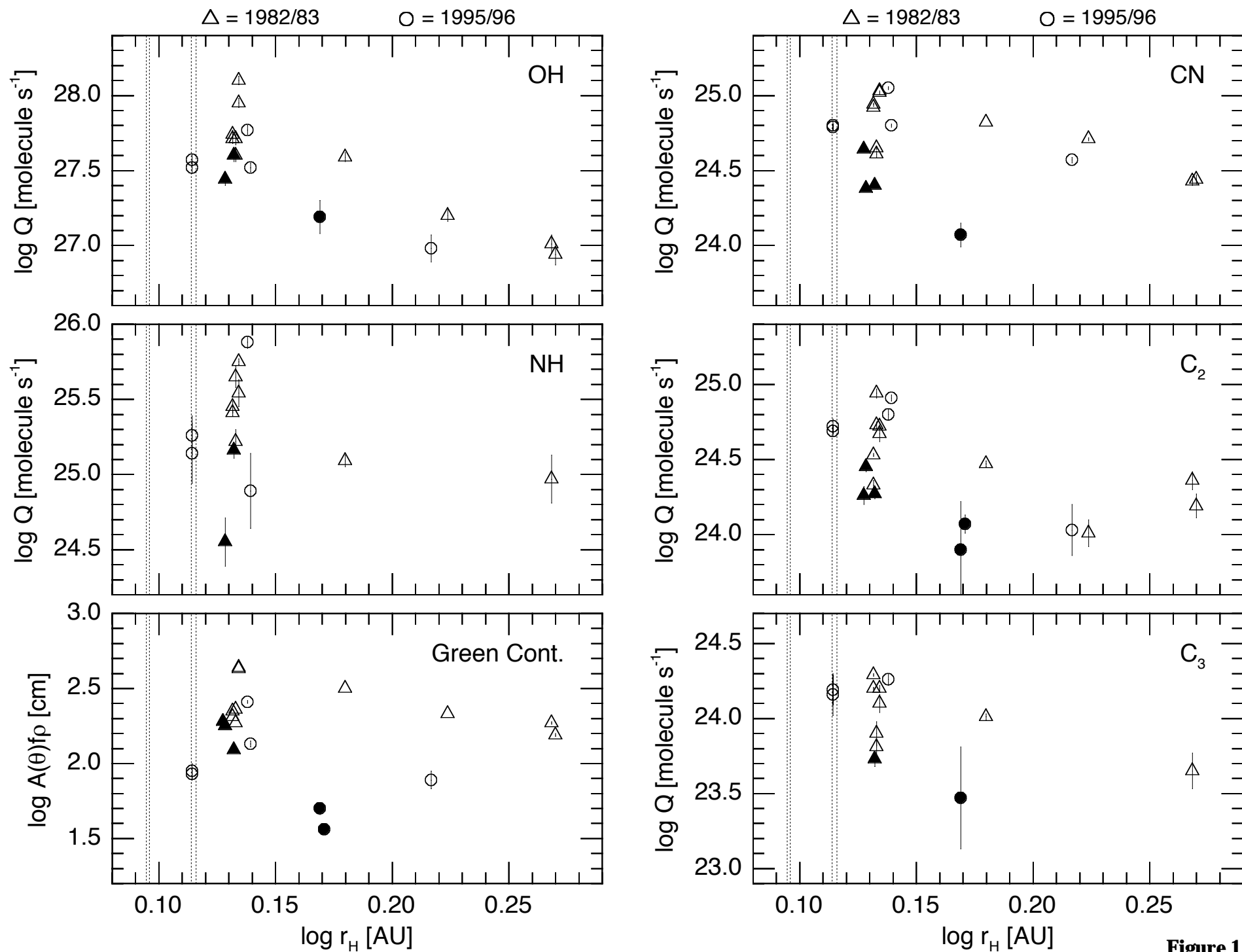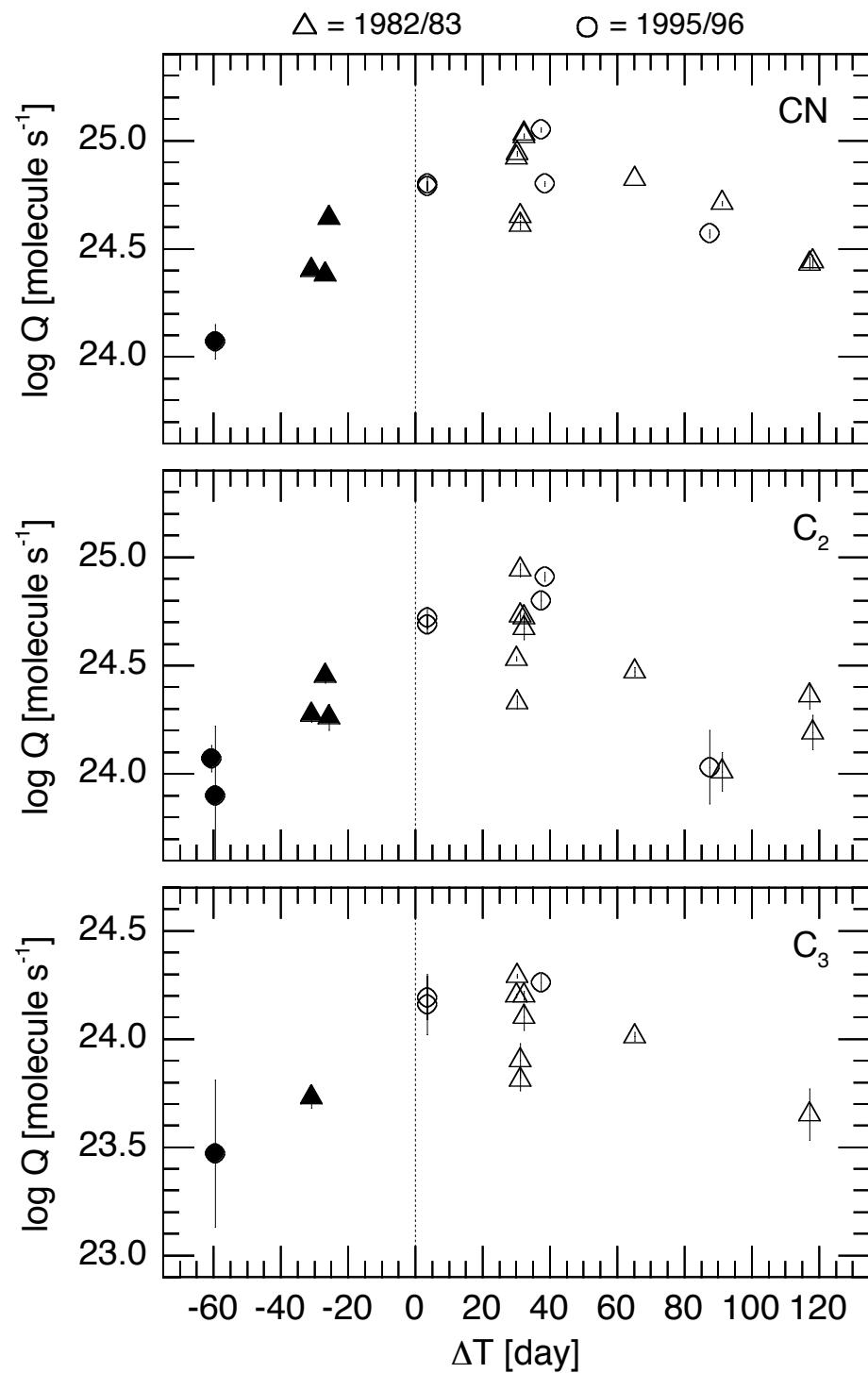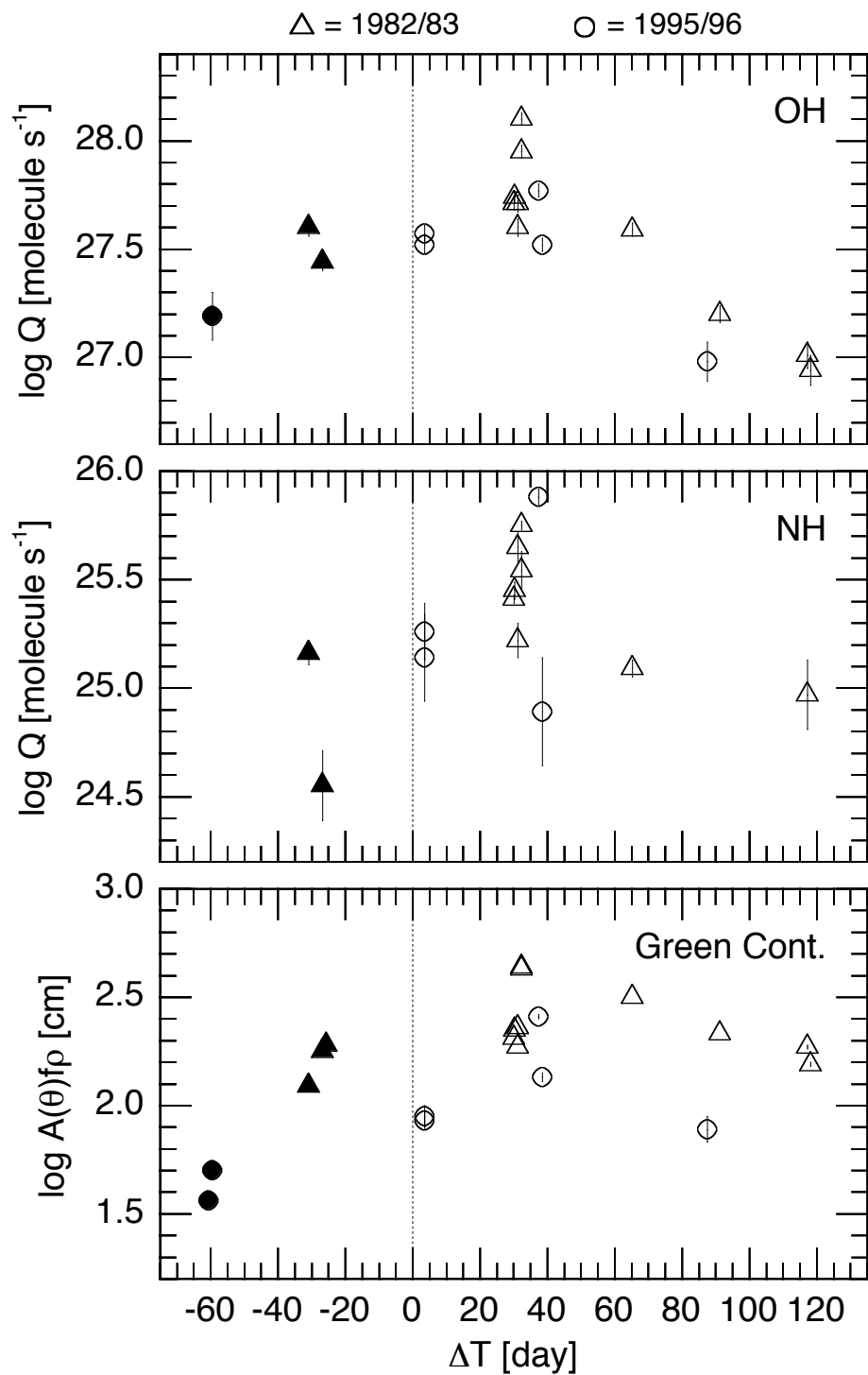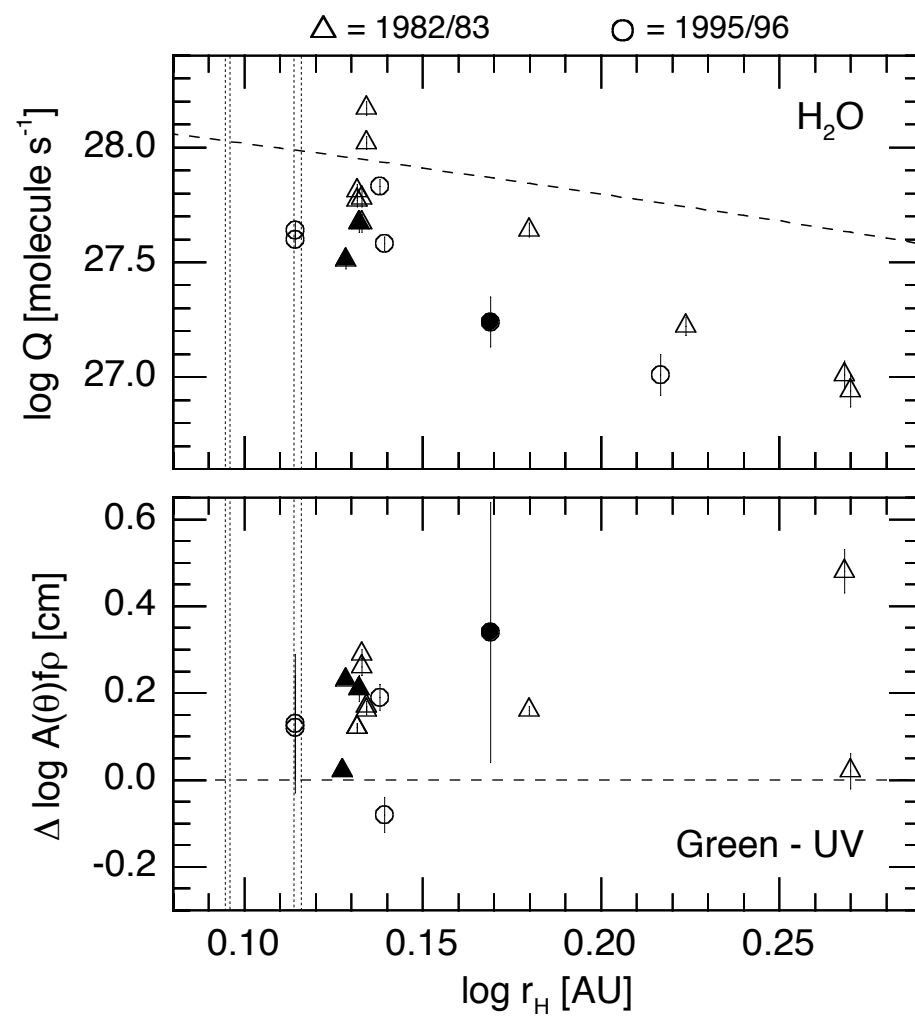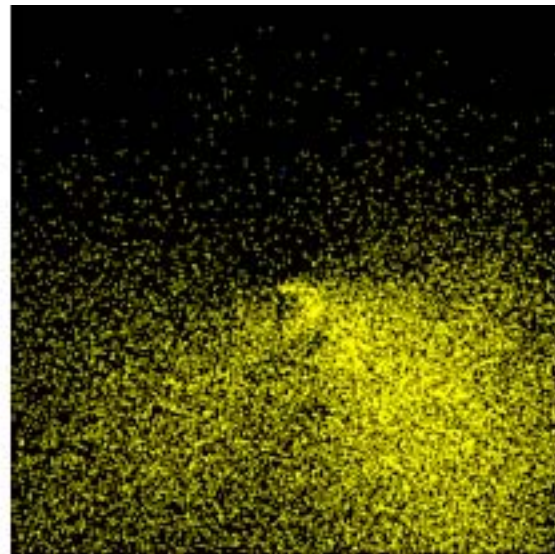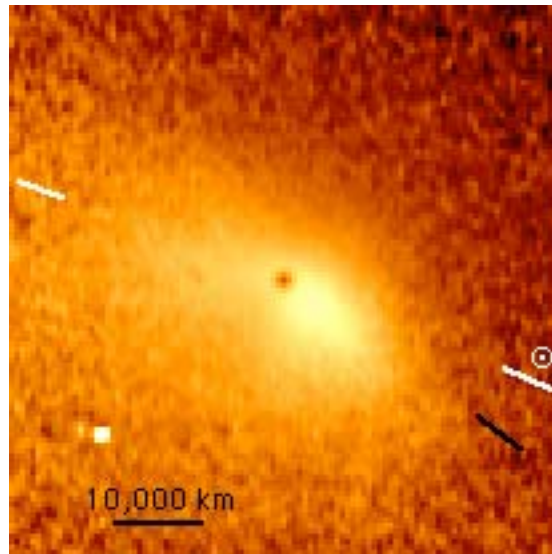
Figure 1

Figure 2

Figure 3

Figure 4
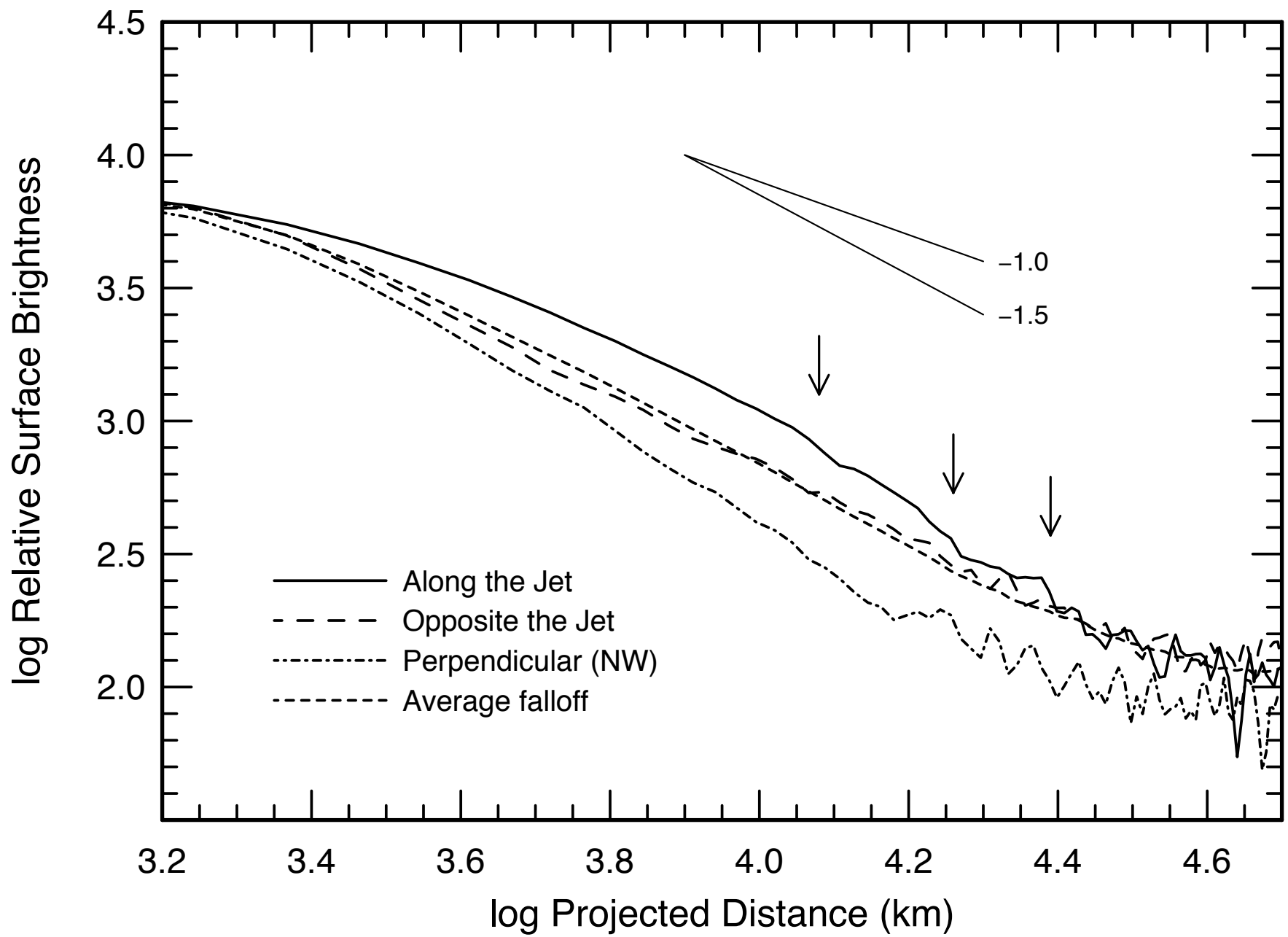
Figure 5

TABLE 1

Observing Circumstances and Fluorescence Efficiencies

for Comet 67P/Churyumov-Gerasimenko

UT Date	ΔT (day)	r_H (AU)	Δ (AU)	Phase Angle (°)	PA of Sun (°)	$\dot{r}_H$ (km s^{-1})	log L/N^a (erg s^{-1} molecule^{-1}) OH	NH	CN	Inst
1982 Oct 12.32	−30.777	1.356	0.516	37.5	NA	−5.5	−14.721	−13.127	−12.435	Phot
1982 Oct 16.43	−26.667	1.344	0.494	37.3	NA	−4.8	−14.718	+13.136	−12.449	Phot
1982 Oct 17.40	−25.698	1.341	0.489	37.2	NA	−4.7	−14.718	−13.137	−12.451	Phot
1982 Dec 12.26	+30.160	1.354	0.403	19.9	NA	+5.4	−14.540	−13.264	−12.336	Phot
1982 Dec 12.29	+30.192	1.354	0.403	19.9	NA	+5.4	−14.540	−13.264	−12.336	Phot
1982 Dec 13.29	+31.193	1.358	0.405	19.4	NA	+5.6	−14.536	−13.260	−12.333	Phot
1982 Dec 13.32	+31.216	1.358	0.405	19.4	NA	+5.6	−14.536	−13.260	−12.333	Phot
1982 Dec 14.48	+32.377	1.362	0.408	18.8	NA	+5.7	−14.534	−13.259	−12.332	Phot
1982 Dec 14.52	+32.417	1.362	0.408	18.8	NA	+5.7	−14.534	−13.259	−12.332	Phot
1983 Jan 16.40	+65.297	1.513	0.552	13.3	NA	+9.8	−14.468	−13.213	−12.331	Phot
1983 Feb 11.31	+91.208	1.674	0.784	21.5	NA	+11.6	−14.339	−13.208	−12.364	Phot
1983 Mar 9.25	+117.149	1.855	1.116	26.6	NA	+12.5	−14.274	−13.210	−12.392	Phot
1983 Mar 10.24	+118.137	1.862	1.130	26.7	NA	+12.5	−14.274	−13.210	−12.393	Phot
1995 Nov 18.10	−60.563	1.482	0.962	41.2	NA	−9.4	−14.661	−13.150	−12.442	Phot
1995 Nov 19.20	−59.463	1.476	0.964	41.5	NA	−9.3	−14.671	−13.147	−12.439	Phot
1996 Jan 21.12	+3.458	1.301	1.095	47.6	NA	+0.7	−14.817	−13.288	−12.573	Phot
1996 Jan 21.13	+3.473	1.301	1.095	47.6	NA	+0.7	−14.817	−13.288	−12.573	Phot
1996 Jan 25.19	+7.528	1.303	1.109	47.3	248.0	NA	NA	NA	NA	CCD
1996 Feb 24.12	+37.465	1.374	1.264	43.8	NA	+6.6	−14.568	−13.243	−12.326	Phot
1996 Feb 25.15	+38.490	1.378	1.271	43.6	NA	+6.7	−14.567	−13.242	−12.326	Phot
1996 Apr 14.21	+87.545	1.647	1.765	34.0	NA	+11.5	−14.388	−13.208	−12.360	Phot

[a] Fluorescence efficiencies are for r_H = 1 AU, and are scaled by r_H^{-2} in the reductions.

TABLE 2

Photometric Fluxes and Column Abundances for Comet 67P/Churyumov-Gerasimenko

UT Date	Aperture Size (arcsec)	log ρ (km)	log Emission Band Flux (erg cm^{-2} s^{-1}) OH	NH	CN	C$_3$	C$_2$	log Cont. Flux[a] (erg cm^{-2} s^{-1} Å^{-1}) UV	Green	log M(ρ) (molecule) OH	NH	CN	C$_3$	C$_2$
1982 Oct 12.32	37.8	3.85	−11.01	−12.11	−11.73	−11.66	−11.98	−13.84	−13.44	30.85	28.15	27.84	27.48	27.51
1982 Oct 16.43	19.5	3.54	−11.64	−13.22	−12.22	—	−12.26	−13.96	−13.54	30.17	27.01	27.32	—	27.18
1982 Oct 17.40	13.7	3.39	—	—	−12.22	—	−12.71	−13.86	−13.66	—	—	27.31	—	26.72
1982 Dec 12.26	38.9	3.75	−10.67	−11.95	−11.05	−11.09	−11.66	−13.41	−13.10	30.79	28.24	28.20	27.83	27.61
1982 Dec 12.29	19.5	3.45	−11.15	−12.43	−11.54	−11.44	−12.37	−13.67	−13.35	30.31	27.76	27.72	27.49	26.90
1982 Dec 13.29	13.7	3.30	−11.57	−12.94	−12.10	−12.16	−12.24	−13.98	−13.50	29.90	27.25	27.17	26.77	27.04
1982 Dec 13.32	6.9	3.01	−11.99	−13.05	−12.66	−12.56	−12.56	−14.34	−13.89	29.48	27.14	26.61	26.37	26.72
1982 Dec 14.48	27.6	3.61	−10.68	−11.88	−11.20	−11.32	−11.73	−13.29	−12.93	30.79	28.32	28.07	27.62	27.56
1982 Dec 14.52	13.7	3.31	−11.07	−12.63	−11.73	−11.88	−12.30	−13.59	−13.22	30.41	27.57	27.54	27.06	26.98
1983 Jan 16.40	38.9	3.89	−10.92	−12.42	−11.35	−11.51	−11.92	−13.49	−13.14	30.84	28.09	28.27	27.79	27.71
1983 Feb 11.31	19.5	3.74	−11.89	—	−12.19	—	−13.09	—	−13.85	30.14	—	27.86	—	26.94
1983 Mar 9.25	19.5	3.90	−12.21	−13.44	−12.69	−12.71	−12.93	−14.82	−14.15	30.14	27.85	27.78	27.37	27.50
1983 Mar 10.24	19.5	3.90	−12.28	—	−12.70	—	−13.11	−14.45	−14.24	30.09	—	27.79	—	27.33
1995 Nov 18.10	75.3	4.42	—	—	—	—	−11.95	—	−14.00	—	—	—	—	28.16
1995 Nov 19.20	52.8	4.27	−11.35	—	−12.07	−12.06	−12.34	−14.59	−14.01	31.07	—	28.13	27.69	27.76
1996 Jan 21.12	109.7	4.64	−10.52	−11.60	−10.92	−11.11	−10.96	−13.75	−13.39	32.05	29.44	29.41	28.65	29.14
1996 Jan 21.13	109.7	4.64	−10.56	−11.49	−10.93	−11.08	−10.99	−13.77	−13.41	32.01	29.56	29.40	28.68	29.11
1996 Feb 24.12	26.5	4.08	−11.10	−11.90	−11.39	−11.64	−11.86	−14.08	−13.65	31.40	29.27	28.86	28.29	28.42
1996 Feb 25.15	37.8	4.24	−11.11	−12.64	−11.41	—	−11.52	−13.94	−13.79	31.40	28.53	28.85	—	28.77
1996 Apr 14.21	106.4	4.83	−11.11	—	−11.37	—	−12.08	—	−13.87	31.65	—	29.37	—	28.65

[a] Continuum filter wavelengths: UV (1982/83) = 3675 Å; UV (1995/96) = 3650 Å; Green (1982/83) = 5240 Å; Green (1995/96) = 4845 Å.

TABLE 3

Photometric Production Rates for Comet 67P/Churyumov-Gerasimenko

UT Date	ΔT (day)	$\log r_H$ (AU)	$\log \rho$ (km)	$\log Q^a$ (molecule s^{-1}) OH	NH	CN	C_3	C_2	$\log A(\theta)f\rho^{a,b}$ (cm) UV	Green	$\log Q$ H$_2$O
1982 Oct 12.32	−30.777	0.132	3.85	27.60 .04	25.16 .05	24.40 .01	23.73 .05	24.27 .03	1.88 .03	2.09 .01	27.67
1982 Oct 16.43	−26.667	0.128	3.54	27.44 .04	24.55 .16	24.38 .01	—	24.45 .03	2.02 .01	2.25 .00	27.51
1982 Oct 17.40	−25.698	0.127	3.39	—	—	24.64 .01	—	24.26 .06	2.26 .01	2.28 .00	0.00
1982 Dec 12.26	+30.160	0.132	3.75	27.71 .03	25.41 .02	24.92 .00	24.20 .01	24.53 .01	2.19 .01	2.31 .00	27.77
1982 Dec 12.29	+30.192	0.132	3.45	27.74 .03	25.45 .04	24.94 .01	24.29 .01	24.33 .03	2.23 .01	2.35 .00	27.81
1982 Dec 13.29	+31.193	0.133	3.30	27.60 .04	25.22 .08	24.65 .01	23.81 .05	24.73 .02	2.07 .01	2.36 .00	27.67
1982 Dec 13.32	+31.216	0.133	3.01	27.71 .04	25.65 .07	24.61 .02	23.90 .08	24.94 .03	2.01 .02	2.27 .00	27.78
1982 Dec 14.48	+32.377	0.134	3.61	27.95 .03	25.75 .02	25.03 .00	24.20 .02	24.72 .02	2.47 .01	2.63 .00	28.02
1982 Dec 14.52	+32.417	0.134	3.31	28.10 .03	25.54 .09	25.02 .01	24.10 .06	24.67 .05	2.47 .01	2.64 .00	28.17
1983 Jan 16.40	+65.297	0.180	3.89	27.59 .03	25.09 .04	24.82 .00	24.01 .02	24.47 .02	2.34 .01	2.50 .00	27.64
1983 Feb 11.31	+91.208	0.224	3.74	27.20 .04	—	24.71 .01	—	24.01 .09	—	2.33 .00	27.22
1983 Mar 9.25	+117.149	0.268	3.90	27.01 .06	24.97 .16	24.43 .03	23.65 .12	24.36 .06	1.79 .05	2.27 .01	27.01
1983 Mar 10.24	+118.137	0.270	3.90	26.94 .07	—	24.44 .03	—	24.19 .08	2.17 .04	2.19 .01	26.94
1995 Nov 18.10	−60.563	0.171	4.42	—	—	— .00	—	24.07 .06	—	1.56 .03	0.00
1995 Nov 19.20	−59.463	0.169	4.27	27.19 .11	—	24.07 .08	23.47 .34	23.90 .32	1.36 .30	1.70 .04	27.24
1996 Jan 21.12	+3.458	0.114	4.64	27.57 .04	25.14 .20	24.80 .03	24.16 .14	24.72 .05	1.82 .16	1.95 .05	27.64
1996 Jan 21.13	+3.473	0.114	4.64	27.52 .04	25.26 .13	24.79 .02	24.19 .10	24.69 .04	1.81 .12	1.93 .04	27.60
1996 Feb 24.12	+37.465	0.138	4.08	27.77 .03	25.88 .04	25.05 .01	24.26 .04	24.80 .04	2.22 .03	2.41 .01	27.83
1996 Feb 25.15	+38.490	0.139	4.24	27.52 .03	24.89 .25	24.80 .01	—	24.91 .02	2.21 .04	2.13 .02	27.58
1996 Apr 14.21	+87.545	0.217	4.83	26.98 .09	—	24.57 .02	—	24.03 .17	—	1.89 .06	27.01

[a] Production rates, followed by uncertainties.

[b] Continuum filter wavelengths: UV (1982/83) = 3675 Å; UV (1995/96) = 3650 Å; Green (1982/83) = 5240 Å; Green (1995/96) = 4845 Å.

TABLE 4

Heliocentric Distance Dependencies and Abundance Ratios

for Comet 67P/Churyumov-Gerasimenko

Species	r_H–Dependence			log Production Rate
	Pre-Perihelion[a]	Post-Perihelion[b]	Post-Perihelion[c]	Ratios (X/OH)
OH	–6.4±2.1	–5.4±1.0	–6.3±0.9	0.00
NH	–16.4±21.3	–3.0±2.2	–4.2±2.3	–2.35±.26
CN	–13.1±2.6	–2.7±0.7	–3.1±0.8	–2.82±.23
C_3	–12.8±2.9	–3.3±1.1	–3.3±1.3	–3.62±.21
C_2	–11.7±2.3	–4.1±1.0	–4.2±1.2	–3.02±.26
UV Cont.	–9.5±5.6	–0.6±1.3	–1.7±1.1	–25.49±.26[d]
Green Cont.	–8.0±3.6	–0.4±1.2	–1.6±1.0	–25.27±.27[d]

[a] For pre-perihelion and $\Delta T = +3$ day data.

[b] For all post-perihelion data.

[c] For post-perihelion, excluding $\Delta T = +3$ day data.

[d] For the dust continuum, the ratio of $A(\theta)f\rho$ to Q(OH) has units of cm sec mol^{-1}.